

Control of a Two-Dimensional Electron Gas on SrTiO₃(111) by Atomic Oxygen

S. McKeown Walker,¹ A. de la Torre,¹ F. Y. Bruno,¹ A. Tamai,¹ T. K. Kim,² M. Hoesch,² M. Shi,³
M. S. Bahramy,^{4,5} P. D. C. King,⁶ and F. Baumberger^{1,3,6}

¹Département de Physique de la Matière Condensée, Université de Genève, 24 Quai Ernest-Ansermet, 1211 Genève 4, Switzerland

²Diamond Light Source, Harwell Campus, Didcot OX11 0DE, United Kingdom

³Swiss Light Source, Paul Scherrer Institut, CH-5232 Villigen PSI, Switzerland

⁴Quantum-Phase Electronics Center, Department of Applied Physics, The University of Tokyo, Tokyo 113-8656, Japan

⁵RIKEN Center for Emergent Matter Science (CEMS), Wako 351-0198, Japan

⁶SUPA, School of Physics and Astronomy, University of St Andrews, St Andrews, Fife KY16 9SS, United Kingdom

(Received 12 May 2014; published 20 October 2014)

We report on the formation of a two-dimensional electron gas (2DEG) at the bare surface of (111) oriented SrTiO₃. Angle resolved photoemission experiments reveal highly itinerant carriers with a sixfold symmetric Fermi surface and strongly anisotropic effective masses. The electronic structure of the 2DEG is in good agreement with self-consistent tight-binding supercell calculations that incorporate a confinement potential due to surface band bending. We further demonstrate that alternate exposure of the surface to ultraviolet light and atomic oxygen allows tuning of the carrier density and the complete suppression of the 2DEG.

DOI: 10.1103/PhysRevLett.113.177601

PACS numbers: 79.60.Bm, 73.20.-r, 73.21.Fg

The emergent field of oxide electronics relies on the creation and manipulation of interface electronic states. Following the seminal discovery of a high mobility two-dimensional electron gas (2DEG) at the (001) interface between the perovskite band insulators SrTiO₃ (STO) and LaAlO₃ (LAO) [1], much work has been devoted to revealing its unique properties, including gate controlled metal-insulator transitions [2], superconductivity [3], and its possible coexistence with magnetism [4]. Notably, 2DEGs in STO(001) can be created by very different means, such as bombardment of STO single crystals by Ar⁺ ions [5], electrolyte gating [6], or deposition of amorphous [7] and non-perovskite oxides [8]. Yet, the resulting surface and interface 2DEGs all display similar electronic transport phenomena, suggesting a common underlying electronic structure defined by the properties of STO and the crystallographic orientation of the surface or interface (see Fig. 1). Angle resolved photoemission (ARPES) experiments on the bare STO(001) surface [9–11] indeed indicate a crucial role of the confinement direction in shaping key properties of the 2DEG there, such as orbital ordering and, related to this, an unconventional Rashba splitting, possibly driving the marked density dependence of magnetotransport phenomena in STO(001) 2DEGs [11–17]. Yet, the origin of surface 2DEGs on STO remains highly controversial [9,10,18,19].

Recent theoretical work suggests that (111) oriented ABO₃ perovskites might display particularly intriguing phenomena. Along this direction a bilayer of B-site ions forms a honeycomb lattice (see Fig. 1), potentially suitable for realizing novel topological phases [20–22]. Moreover, thin quantum wells of STO(111) were predicted to be ferromagnetic and/or ferroelectric [23]. However, despite

the successful creation of 2DEGs at the (111)-oriented interface of STO/LAO [24] and at the bare surface of KTaO₃ [22], little is known to date from experiment about their origin and microscopic electronic structure.

Here we use angle resolved photoemission to show that the *in situ* cleaved (111) surface of SrTiO₃ [25] supports a robust, quantum confined two-dimensional

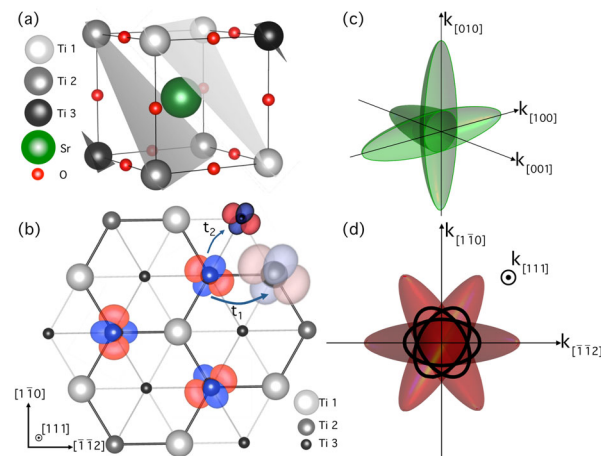


FIG. 1 (color online). (a) Schematic of a cubic perovskite unit cell of SrTiO₃ with inequivalent (111) planes indicated in grey. (b) Top view of three consecutive Ti⁴⁺ (111) layers. Each of the three t_{2g} orbitals is shown on the honeycomb lattice, formed by two consecutive layers (dark grey lines), to illustrate their rotational symmetry. The xz orbital is shown in all three layers with large (t_1) and small (t_2) nearest neighbor hoppings indicated. (c) Sketch of the bulk FS of STO cut by the (001) plane. (d) The same bulk FS viewed down the [111] axis. A cut in the (111) plane through the Γ point is indicated by black lines to illustrate its different shape and size from the projection of the FS on the (111) surface plane.

electron system. Our model calculation fully reproduces the observed electronic structure and describes how the 2DEG emerges from the quantum confinement of t_{2g} electrons near the surface due to band bending. Moreover, we demonstrate how the 2DEG can be reversibly depleted and created by alternately exposing the surface to low doses of atomic oxygen and ultraviolet (UV) light.

Single crystals of commercially grown (Crystal GmbH), lightly electron doped $\text{SrTi}_{1-x}\text{Nb}_x\text{O}_3(111)$ ($x = 0.002$) were measured. The Nb doping results in a small residual bulk conductivity and a maximum doping of $3 \times 10^{19} \text{ cm}^{-3}$, which helps to eliminate charging effects during ARPES but does not otherwise influence our results. Samples were cleaved at a pressure lower than 5×10^{-10} mbar at the measurement temperature. ARPES measurements ($T = 20 \text{ K}$, $h\nu = 40\text{--}140 \text{ eV}$) were performed at the SIS beam line of the Swiss Light Source and the I05 beam line of the Diamond Light Source with an angular resolution of $\approx 0.2^\circ$ and an energy resolution of 10–20 meV.

The ARPES Fermi surface (FS) of $\text{STO}(111)$ shown in Fig. 2(a) consists of three equivalent elliptical sheets oriented along $\bar{\Gamma}\bar{M}$ [26]. The band structure along $\bar{\Gamma}\bar{M}$ [Fig. 2(b)] shows a single heavy band, corresponding to the long axis of one of the FS ellipses, which is nearly degenerate at the band bottom with a more dispersive, doubly degenerate band arising from the two remaining FS sheets. Near the Fermi level, additional dispersive spectral weight is observed, indicating a second occupied subband, which is a natural consequence of quantum confinement and is not observed in the bulk. From the FS area we deduce a 2D carrier density of $1.5 \times 10^{14} \text{ cm}^{-2}$. Assuming a constant electron density over approximately 15 Ti layers (33 Å) below the surface [which is consistent with the computational results shown

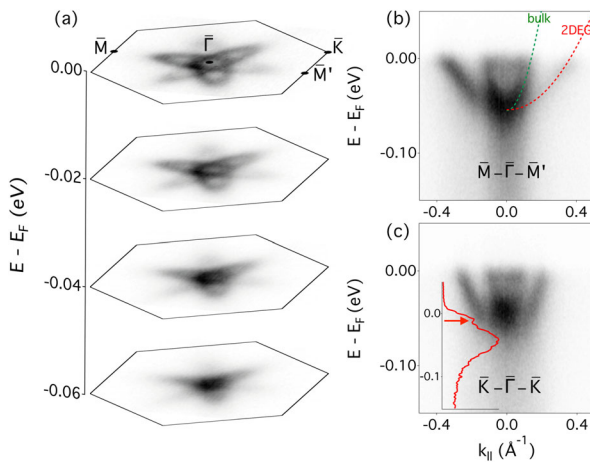


FIG. 2 (color online). (a) Constant energy surfaces of the $\text{STO}(111)$ electronic structure measured at 108 eV with circularly polarized light. (b),(c) Energy—momentum dispersion along two high-symmetry directions (108 eV, p polarization). A calculation (fit) of the bulk (2DEG) dispersion in the same direction is indicated by green (red) dashed lines, in (b). Inset of (c) is an energy distribution curve at $\bar{\Gamma}$, the red arrow indicates the peak due to the second subband.

in Fig. 3(b)], this corresponds to a 3D density at the surface of $4.5 \times 10^{20} \text{ cm}^{-3}$, more than an order of magnitude higher than the nominal bulk doping of our samples. We also confirmed the 2D nature of the charge carriers directly through extensive photon energy dependent measurements, which reveal no signs of dispersion along k_z within the accuracy of the experiment (see Supplemental Material [27]). Together, these observations conclusively demonstrate that the observed electronic structure arises from quantum confinement in a surface 2DEG.

Although the strongly polar (111) surface of STO likely reconstructs following cleavage in vacuum [28,29], we find no evidence for backfolded bands over a wide photon energy range and over multiple Brillouin zones. This is consistent with recent findings on $\text{STO}(110)$ [30] and indicates that the 2DEG wave functions have a negligible weight in the topmost Ti layer where the in-plane potential from a possible surface reconstruction is strongest. We further do not observe a lifting of the spin degeneracy in the 2DEG within the resolution of our experiment. From the observed line widths, we can estimate an upper limit of $\approx 15 \text{ meV}$ for a possible Rashba or exchange splitting, more than an order of magnitude smaller than predicted for thin quantum wells of $\text{STO}(111)$ [23].

Intriguingly, the FS ellipses we observe are elongated with respect to those of our bulk electronic structure calculations in the (111) plane. From fits to the measured dispersion, we find a band mass of $\bar{m}_H \approx 8.7 m_e$ for the long axis of the FS ellipses, nearly 6 times higher than the calculated bulk

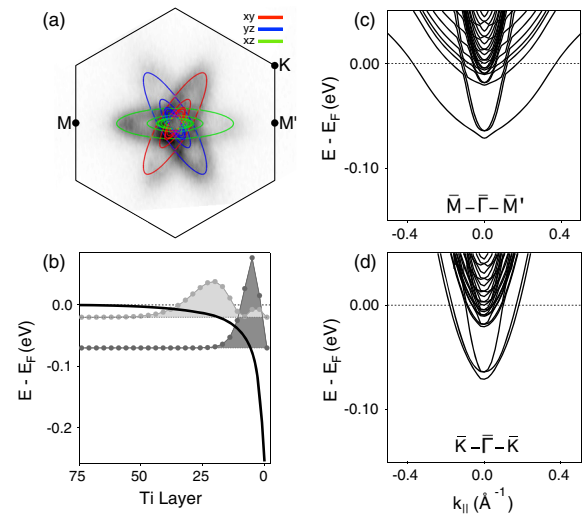


FIG. 3 (color online). Tight-binding supercell calculations of the electronic structure at the (111) surface of SrTiO_3 . (a) The calculated FS and orbital character superposed on the ARPES data. (b) The self-consistent band bending potential. One Ti layer corresponds to 2.25 Å. The square modulus of the wave functions of the lowest two subbands at $\bar{\Gamma}$ are plotted at their corresponding confinement energies. (c),(d) Calculated band dispersion along two high-symmetry directions, showing three confined 2DEG subbands and a “ladder” of states above E_F due to the finite size of the supercell.

mass along the same crystallographic direction, in stark contrast to the case of the STO(001) 2DEG, where the band masses are similar to the bulk. At first sight, it is tempting to assign the large mass renormalization in the 2DEG to enhanced electron correlations as the system evolves with increasing density from the weakly correlated d^0 configuration of undoped SrTiO₃ towards the strongly correlated d^1 state of the Mott insulator LaTiO₃. However, as we will show later, the marked renormalization is more naturally explained as a nontrivial consequence of quantum confinement and thus does not provide evidence for pronounced many-body effects.

We first discuss the experimental findings on a qualitative level. Since in a 2D system the electronic states have the same energy for all values of the momentum k_z perpendicular to the surface, the Fermi surface of the 2DEG can be approximated by a projection of the 3D bulk band structure (at appropriate doping levels) onto the surface plane. In the case of STO(001), the surface projection is identical to a cut through the bulk FS as is evident from the sketch in Fig. 1(c). Consequently, the band masses of the 2DEG closely resemble those of the bulk calculations. In contrast, a projection onto the (111) plane results in elliptical contours that are strongly elongated compared to a cut through the bulk FS as demonstrated in Fig. 1(d), consistent with our observation of enhanced effective masses. The degeneracy of the bands can be understood by considering the different symmetry and atomic arrangement of STO(111) and STO(001) surfaces illustrated in Fig. 1. While the xy and xz/yz orbitals have very different overlap along the [001] confinement direction of STO(001), all t_{2g} orbitals are equivalent modulo a rotation of 120° when viewed along the surface normal of STO(111) [see Fig. 1(b)]. This immediately suggests that quantum confinement will not drive a significant orbital polarization in the STO(111) 2DEG, in stark contrast to STO(001) [11,13,14,31,32], which is indeed what we observe experimentally.

This qualitative understanding is supported by tight-binding supercell calculations based on a nonrelativistic *ab initio* bulk band structure. To calculate the surface electronic structure, a supercell containing 120 Ti atoms stacked along the [111] direction was constructed using maximally localized Wannier functions with additional on-site potential terms to account for band bending via an electrostatic potential variation. The tight-binding Hamiltonian was solved self-consistently with Poisson's equation, incorporating an electric field dependent dielectric constant [11,33,34]. The only adjustable parameter is the total magnitude of the band bending at the surface, which we choose to reproduce the experimentally observed binding energy of the lowest subband (≈ 60 meV). This band bending requires the presence of a layer of positive charge at the surface, which we will later attribute to oxygen vacancies. Other than this, the calculation assumes a bulk truncated (111) surface devoid of any reconstructions.

The results of this calculation, shown in Fig. 3, clearly reproduce the experimentally observed band dispersion and

Fermi surface of the lowest subband. They further indicate a ladder of three higher subbands with progressively more bulklike character. The second subband is predicted just below the Fermi energy, again in good agreement with the experiment. The wave functions of the lowest subband at $\bar{\Gamma}$ extend over ≈ 15 Ti layers (33 Å), and thus nearly an order of magnitude more than the bulk penetration of the first xy subband on STO(001) [11]. This can be attributed to the lighter effective mass perpendicular to the surface and the correspondingly shallower binding energy. The diminishing weight of the wave function in the topmost Ti layer further justifies the assumption of a bulk-truncated surface for the modeling of the electronic structure.

For the remainder of this Letter, we discuss the origin of the 2DEG and its relation to interface 2DEGs. Since STO is a band insulator, charge carriers and appropriate electrostatic boundary conditions, namely, band bending, are needed to create a 2DEG. In the ideal polar catastrophe scenario for LAO/STO(001), both are provided by the intrinsic electric field in the LAO layer, which allows separation of electrons and holes, resulting in electron accumulation in STO and doped holes on the surface of LAO. While there is strong experimental evidence for this scenario in the case of LAO/STO(001) [35,36], it clearly cannot apply to a bare STO surface.

Experimentally, we observe that the 2DEG develops on the STO(111) surface only after exposure to intense UV radiation, just as for the 2DEG of STO(001) [9,11], indicating a common microscopic origin of the quantum confined charge carriers on both surfaces. For the case of STO(001), we proposed earlier that light-induced oxygen desorption [37] might drive the formation of the 2DEG [9], but this remained controversial [10,18]. At low temperature, vacancy diffusion will be strongly suppressed and oxygen desorption will be limited to the topmost layer. The system will then try to screen the positively charged vacancies with mobile carriers, which requires band bending such that the edge of the conduction band is dragged below the Fermi level in a narrow layer at the surface.

To test this hypothesis we exposed the cleaved surface of STO at low temperature (≈ 8 K) alternately to UV light and atomic oxygen while monitoring the presence of the 2DEG and changes in the O 2*p* valence bands. The angle integrated photoemission spectra of the surface after illumination with the synchrotron UV beam ($h\nu = 108$ eV, $\approx 10^{15}$ photons $s^{-1} mm^{-2}$) for ≈ 1 h (black) and immediately after exposure to atomic oxygen (green) are shown in Fig. 4(a) [38]. The main features of the spectra are the sharp 2DEG peak just below the Fermi level, the O 2*p* valence band with an onset near -3 eV and an in-gap state around -1.3 eV, which was attributed to oxygen vacancies in Refs. [39–41]. Upon exposure to atomic oxygen the 2DEG peak and the in-gap defect state completely vanish, and concomitant with the depletion of the 2DEG, the VB leading edge midpoint [LEM] shifts towards the Fermi level by ≈ 300 meV. Assuming a constant band gap, this

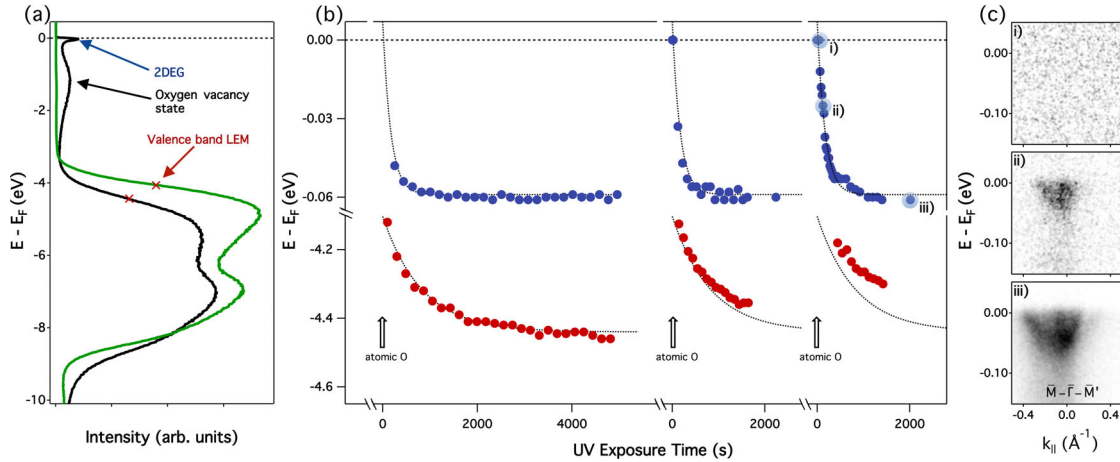


FIG. 4 (color online). Atomic oxygen treatment of the cleaved STO(111) surface. (a) Angle integrated photoemission spectra from a surface with a fully developed (suppressed) 2DEG after UV (atomic oxygen) [black (green)] exposure. (b) Occupied bandwidth of the 2DEG (blue) and valence band leading-edge midpoint (red) as a function of time exposed to UV radiation after atomic oxygen exposure which is indicated by arrows and marked by a break in the time axis. The dashed black lines are guides to the eye. Zero bandwidth indicates complete suppression of the 2DEG. (c) Dispersion plots in the $\bar{M}'\text{-}\bar{\Gamma}\text{-}\bar{M}'$ direction from three stages of the 2DEG development as indicated in panel (b).

implies a strongly reduced or vanishing band bending following exposure to atomic oxygen. We note that the exact magnitude of the surface band bending is difficult to extract from such data since the photoemission probing depth is comparable to the width of surface band bending. The VB peak will thus contain contributions from unit cells with locally different band energies.

Figure 4(b) shows the systematic time evolution of the valence band leading edge and the occupied 2DEG bandwidth as the surface is repeatedly exposed to atomic oxygen and UV radiation. The data clearly show that the onset of band bending coincides with near-surface charge accumulation and that both the bandwidth of the 2DEG and the depth of the confining potential saturate at long time [42]. In parallel with this, the in-gap state loses all spectral weight when the surface is treated with atomic oxygen, consistent with the filling of all oxygen vacancies, and recovers as the surface is irradiated again. In Fig. 4(c) we show three dispersion plots obtained after the third consecutive exposure to atomic oxygen. Immediately after oxygen exposure the surface is insulating and no spectral weight is observed at the Fermi level. After ≈ 100 s UV exposure a 2DEG with an occupied bandwidth around 30 meV develops. Following longer exposure to UV light, the 2DEG fully recovers the bandwidth and Fermi wave vector of samples that were not treated with atomic oxygen. This indicates that the electronic structure of the 2DEG is largely defined by the electrostatic boundary conditions controlled by the density of charged oxygen vacancies on the surface and is remarkably insensitive to the detailed atomic structure of the surface, which likely changes after exposure to atomic oxygen. We attribute this to the spatial extent of the wave function, which has little weight in the topmost plane and peaks around 6 Ti layers below the surface [see Fig. 3(b)]. We note that annealing of LAO/STO (001) samples in atomic oxygen reduces the

amount of oxygen vacancies in the heterostructure but does not suppress the 2DEG [43]. The absence of an LAO overlayer in our case allows us to achieve the full depletion of the 2DEG.

Together, our observations conclusively demonstrate that the STO(111) surface supports a 2DEG with sixfold symmetry, which is quantum confined by a band bending potential induced by surface oxygen vacancies. We further demonstrated control of the 2DEG bandwidth by alternate exposure of the surface to UV light and atomic oxygen providing a broadly applicable route to controlling the carrier density and thus the macroscopic properties of transition metal oxide surface 2DEGs.

We gratefully acknowledge discussions with D. Van der Marel and J.-M. Triscone. This work was supported by Swiss National Science Foundation (200021-146995). P.D.C.K. was supported by the UK-EPSC and the Royal Society and M.S.B. by Grant-in-Aid for Scientific Research (S) (No. 24224009) from the Ministry of Education, Culture, Sports, Science and Technology (MEXT) of Japan.

Note added in proof.—After submission of this work we became aware of a related study by Rödel *et al.* [44].

- [1] A. Ohtomo and H. Y. Hwang, *Nature (London)* **427**, 423 (2004).
- [2] A.D. Caviglia, S. Gariglio, N. Reyren, D. Jaccard, T. Schneider, M. Gabay, S. Thiel, G. Hammerl, J. Mannhart, and J.-M. Triscone, *Nature (London)* **456**, 624 (2008).
- [3] N. Reyren, S. Thiel, A. Caviglia, L. F. Kourkoutis, G. Hammerl, C. Richter, C. W. Schneider, T. Kopp, A.-S. Rüetschi, D. Jaccard, M. Gabay, D. A. Muller, J.-M. Triscone, and J. Mannhart, *Science* **317**, 1196 (2007).

- [4] A. Brinkman, M. Huijben, M. van Zalk, J. Huijben, U. Zeitler, J. C. Maan, W. G. van der Wiel, G. Rijnders, D. H. A. Blank, and H. Hilgenkamp, *Nat. Mater.* **6**, 493 (2007).
- [5] D. W. Reagor and V. Y. Butko, *Nat. Mater.* **4**, 593 (2005).
- [6] K. Ueno, S. Nakamura, H. Shimotani, A. Ohtomo, N. Kimura, T. Nojima, H. Aoki, Y. Iwasa, and M. Kawasaki, *Nat. Mater.* **7**, 855 (2008).
- [7] Y. Chen, N. Pryds, J. E. Kleibeuker, G. Koster, J. Sun, E. Stamate, B. Shen, G. Rijnders, and S. Linderth, *Nano Lett.* **11**, 3774 (2011).
- [8] Y. Z. Chen, N. Bovet, F. Trier, D. V. Christensen, F. M. Qu, N. H. Andersen, T. Kasama, W. Zhang, R. Giraud, J. Dufouleur, T. S. Jespersen, J. R. Sun, A. Smith, J. Nygård, L. Lu, B. Büchner, B. G. Shen, S. Linderth, and N. Pryds, *Nat. Commun.* **4**, 1371 (2013).
- [9] W. Meevasana, P. D. C. King, R. H. He, S.-K. Mo, M. Hashimoto, A. Tamai, P. Songsirithigul, F. Baumberger, and Z.-X. Shen, *Nat. Mater.* **10**, 114 (2011).
- [10] A. F. Santander-Syro, O. Copie, T. Kondo, F. Fortuna, S. Pailhès, R. Weht, X. G. Qiu, F. Bertran, A. Nicolaou, A. Taleb-Ibrahimi, P. Le Fèvre, G. Herranz, M. Bibes, N. Reyren, Y. Apert, P. Lecoeur, A. Barthélémy, and M. J. Rozenberg, *Nature (London)* **469**, 189 (2011).
- [11] P. D. C. King, S. McKeown Walker, A. Tamai, A. de la Torre, T. Eknapakul, P. Buaphet, S.-K. Mo, W. Meevasana, M. S. Bahramy, and F. Baumberger, *Nat. Commun.* **5**, 3414 (2014).
- [12] A. Joshua, S. Pecker, J. Ruhman, E. Altman, and S. Ilani, *Nat. Commun.* **3**, 1129 (2012).
- [13] Z. Zhong, A. Tóth, and K. Held, *Phys. Rev. B* **87**, 161102 (2013).
- [14] G. Khalsa, B. Lee, and A. H. MacDonald, *Phys. Rev. B* **88**, 041302 (2013).
- [15] A. Fête, S. Gariglio, A. D. Caviglia, J.-M. Triscone, and M. Gabay, *Phys. Rev. B* **86**, 201105 (2012).
- [16] T. Kimura, J. Hamrle, Y. Otani, K. Tsukagoshi, and Y. Aoyagi, *Appl. Phys. Lett.* **85**, 3795 (2004).
- [17] H. Nakamura, T. Koga, and T. Kimura, *Phys. Rev. Lett.* **108**, 206601 (2012).
- [18] N. C. Plumb, M. Salluzzo, E. Razzoli, M. Månsson, M. Falub, J. Krempasky, C. E. Matt, J. Chang, M. Schulte, J. Braun, H. Ebert, J. Minár, B. Delley, K.-J. Zhou, T. Schmitt, M. Shi, J. Mesot, L. Patthey, and M. Radović, *Phys. Rev. Lett.* **113**, 086801 (2014).
- [19] N. Sivasdas, H. Dixit, V. R. Cooper, and D. Xiao, *Phys. Rev. B* **89**, 075303 (2014).
- [20] D. Xiao, W. Zhu, Y. Ran, N. Nagaosa, and S. Okamoto, *Nat. Commun.* **2**, 596 (2011).
- [21] K.-Y. Yang, W. Zhu, D. Xiao, S. Okamoto, Z. Wang, and Y. Ran, *Phys. Rev. B* **84**, 201104 (2011).
- [22] C. Bareille, F. Fortuna, T. C. Rödel, F. Bertran, M. Gabay, O. H. Cubelos, A. Taleb-Ibrahimi, P. Le Fèvre, M. Bibes, A. Barthélémy, T. Maroutian, P. Lecoeur, M. J. Rozenberg, and A. F. Santander-Syro, *Sci. Rep.* **4**, 3586 (2014).
- [23] D. Doennig, W. E. Pickett, and R. Pentcheva, *Phys. Rev. Lett.* **111**, 126804 (2013).
- [24] G. Herranz, F. Sánchez, N. Dix, M. Scigaj, and J. Fontcuberta, *Sci. Rep.* **2**, 758 (2012).
- [25] Although STO does not have a well-defined cleavage plane the symmetry of measurements from both ARPES and LEED (not shown) indicate that the crystals reproducibly fracture close to the (111) plane.
- [26] Since we observe that the matrix elements of the photoemission process have a lower symmetry when linearly polarized light is used, the data presented in Fig. 2(a) is the sum of spectra taken with right-[C⁺] and left-handed [C⁻] circularly polarized light.
- [27] See Supplemental Material at <http://link.aps.org/supplemental/10.1103/PhysRevLett.113.177601> for details.
- [28] L. D. Marks, A. N. Chiaramonti, F. Tran, and P. Blaha, *Surf. Sci.* **603**, 2179 (2009).
- [29] J. Feng, X. Zhu, and J. Guo, *Surf. Sci.* **614**, 38 (2013).
- [30] Z. Wang, Z. Zhong, X. Hao, S. Gerhold, B. Stöger, M. Schmid, J. Sánchez-Barriga, A. Varykhalov, C. Franchini, K. Held, and U. Diebold, *Proc. Natl. Acad. Sci. U.S.A.* **111**, 3933 (2014).
- [31] Z. S. Popović, S. Satpathy, and R. M. Martin, *Phys. Rev. Lett.* **101**, 256801 (2008).
- [32] M. Salluzzo, J. C. Cezar, N. B. Brookes, V. Bisogni, G. M. De Luca, C. Richter, S. Thiel, J. Mannhart, M. Huijben, A. Brinkman, G. Rijnders, and G. Ghiringhelli, *Phys. Rev. Lett.* **102**, 166804 (2009).
- [33] O. Copie, V. Garcia, C. Bödefeld, C. Carrétéro, M. Bibes, G. Herranz, E. Jacquet, J.-L. Maurice, B. Vinter, S. Fusil, K. Bouzehouane, H. Jaffrès, and A. Barthélémy, *Phys. Rev. Lett.* **102**, 216804 (2009).
- [34] M. S. Bahramy, P. D. C. King, A. de la Torre, J. Chang, M. Shi, L. Patthey, G. Balakrishnan, P. Hofmann, R. Arita, N. Nagaosa, and F. Baumberger, *Nat. Commun.* **3**, 1159 (2012).
- [35] N. Nakagawa, H. Y. Hwang, and D. A. Muller, *Nat. Mater.* **5**, 204 (2006).
- [36] M. L. Reinle-Schmitt, C. Cancellieri, D. Li, D. Fontaine, M. Medarde, E. Pomjakushina, C. W. Schneider, S. Gariglio, P. Ghosez, J.-M. Triscone, and P. R. Willmott, *Nat. Commun.* **3**, 932 (2012).
- [37] M. L. Knotek and P. J. Feibelman, *Phys. Rev. Lett.* **40**, 964 (1978).
- [38] The samples were exposed for ≈ 30 s to a thermal gas cracker operated at ≈ 1700 °C and a flow of 0.004 sccm (1×10^{-7} mbar chamber pressure) resulting in a mixture of $\approx 9\%$ atomic and $\approx 91\%$ molecular oxygen.
- [39] Y. Aiura, I. Hase, H. Bando, T. Yasue, T. Saitoh, and D. S. Dessau, *Surf. Sci.* **515**, 61 (2002).
- [40] F. Lechermann, L. Boehnke, D. Grieger, and C. Piefke, *Phys. Rev. B* **90**, 085125 (2014).
- [41] C. Lin and A. A. Demkov, *Phys. Rev. Lett.* **111**, 217601 (2013).
- [42] To account for a slight angular misalignment in the first run shown in Fig. 4(b), we corrected the VB leading edge midpoint and 2DEG bandwidth by 23 meV and 40 meV, respectively.
- [43] W. Siemons, G. Koster, H. Yamamoto, W. A. Harrison, G. Lucovsky, T. H. Geballe, D. H. A. Blank, and M. R. Beasley, *Phys. Rev. Lett.* **98**, 196802 (2007).
- [44] T. C. Rödel, C. Bareille, F. Fortuna, C. Baumier, F. Bertran, P. Le Fèvre, M. Gabay, O. H. Cubelos, M. J. Rozenberg, T. Maroutian, P. Lecoeur, and A. F. Santander-Syro, *Phys. Rev. Applied* **1**, 051002 (2014).